Engineering *p*-Hydroxyphenylpyruvate Dioxygenase to a *p*-Hydroxymandelate Synthase and Evidence for the Proposed Benzene Oxide Intermediate in Homogentisate Formation†

Michele Gunsior, Jacques Ravel,‡ Gregory L. Challis,§ and Craig A. Townsend*

Department of Chemistry, The Johns Hopkins University, 3400 North Charles Street, Baltimore, Maryland 21218

Received September 30, 2003; Revised Manuscript Received October 29, 2003

ABSTRACT: *p*-Hydroxyphenylpyruvate dioxygenase (HPD) plays a key role in the normal catabolism of tyrosine. An Fe^{2+}/oxygen-dependent enzyme, it converts *p*-hydroxyphenylpyruvate into homogentisate and is part of the superfamily of α-ketoglutarate-dependent enzymes that couples oxidative decarboxylation of an α-ketoacid cofactor to oxidative modification of its substrate. In this case, the α-ketoacid is part of the substrate side chain. HPD shows strong homology to *p*-hydroxymandelate synthase (HMS), an enzyme that catalyzes the formation of *p*-hydroxymandelate from *p*-hydroxyphenylpyruvate, an early step in the biosynthesis of *p*-hydroxyphenylglycine, which is a nonproteinogenic amino acid incorporated into several biologically active secondary metabolites. Sequence alignment between the HPD and the HMS enzyme families and analysis of the *Pseudomonas fluorescens* HPD crystal structure highlighted four residues within each active site that may play roles in catalytic differentiation between the two products. We attempted to convert *Streptomyces avermitilis* HPD into an engineered *S. avermitilis* HMS by site-directed mutagenesis of these four residues individually and in combination. HPLC assay analysis of each His_6-tagged mutant indicated that F337I successfully produced *p*-hydroxymandelate, along with homogentisate and an unknown compound. The structure of the latter was determined to be an oxepinone derived from the benzene-oxide intermediate long hypothesized in HPD catalysis.

p-Hydroxyphenylpyruvate dioxygenase (HPD)[1] carries out one of the most interesting transformations in amino acid catabolism. It catalyzes the oxidative decarboxylation and rearrangement of *p*-hydroxyphenylpyruvate (pHPP) (reversibly formed by transamination of L-tyrosine) to homogentisate (HGA). Further degradation leads ultimately to fumarate and acetate (Scheme 1) (*1*). HPD occupies a central role in the catabolism of aromatic amino acids, and variants have been directly or indirectly involved in a number of metabolic disorders. For example, the hereditary and life-threatening disease tyrosinemia type III is caused by a deficiency in HPD activity (*2*). HPD also catalyzes the first committed step in the synthesis of both plastoquinone and tocopherols, the two major quinone constituents in chloroplasts of higher plants (*3*). Owing to the central role HPD plays in quinone synthesis and tyrosine catabolism, a concerted effort has been made to study this enzyme in various organisms leading to the development of several high affinity inhibitors (*4*−*6*), one of which is used to treat type I tyrosinemia, a fatal disease caused by a 4-fumarylacetoacetate lyase deficiency (*6*). HPD has been purified from a number of organisms including rat (*7*), human (*8*), and pig (*9*), in addition to plants (*10*, *11*), fungi (*12*), and prokaryotes (*13*−*15*). Eukaryotic HPDs behave as homodimers (*1*), whereas in bacteria the enzyme is active as a homotetramer (*15*, *16*).

HPD is a member of the large family of non-heme iron α-ketoglutarate-dependent (α-KG) dioxygenases, which couples oxidation of their substrate to the formation of succinate and CO_2 from α-KG. Unlike most members of this family, however, the α-ketoacid is not a cofactor but part of the substrate itself. Additionally, enzymes in this family show a requirement for ascorbate (*17*), which is believed to keep the active site iron in the reduced, ferrous state necessary for activity. After nearly 50 years of investigation, the mechanism is currently thought to proceed through an oxidative decarboxylation of the pHPP side chain, epoxidation of the aromatic ring, and 1,2-migration of the carboxymethyl side chain in a classic example of the NIH shift to generate the hydroquinone, homogentisate (*1*, *18*, *19*). During the reaction, both atoms of dioxygen are incorporated into the product (*20*), and a hydrogen ortho to the side chain of pHPP is lost (*21*). Some HPD enzymes are also capable of accepting alternate substrates such as 4-fluorophenylpyruvate, and phenylpyruvate, as well as α-ketoisocaproate and β-thiomethyl-α-ketobutyrate to form β-hydroxyisovalerate and thiapentanoate-4-oxide, respectively (*22*, *23*).

† This research was supported by NIH Grants AI 14937 (C.A.T.) and GM 20757 (J.R.) and the Wellcome Trust (G.L.C.).

* To whom correspondence should be addressed. Phone: (410) 516-7444. Fax: (410) 261-1233. E-mail: ctownsend@jhu.edu.

‡ Present address: The Institute for Genomic Research, 9712 Medical Center Dr., Rockville, MD 20850.

§ Present address: Department of Chemistry, University of Warwick, Coventry, UK.

[1] Abbreviations: HPD, *p*-hydroxyphenylpyruvate dioxygenase; HMS, *p*-hydroxymandelate synthase; α-KG, α-ketoglutarate; pHPP, *p*-hydroxyphenylpyruvate; HGA, homogentisate; pHMA, *p*-hydroxymandelate; pHBF, *p*-hydroxybenzoylformate; pHPG, *p*-hydroxyphenylglycine; pHPA, *p*-hydroxyphenylacetate; IPTG, isopropyl β-D-thiogalactopyranoside; CDA, calcium-dependent antibiotic; CD, circular dichroism.

10.1021/bi035762w CCC: $27.50
Published on Web 12/23/2003

Scheme 1: Formation of HGA and pHMA from pHPP[a]

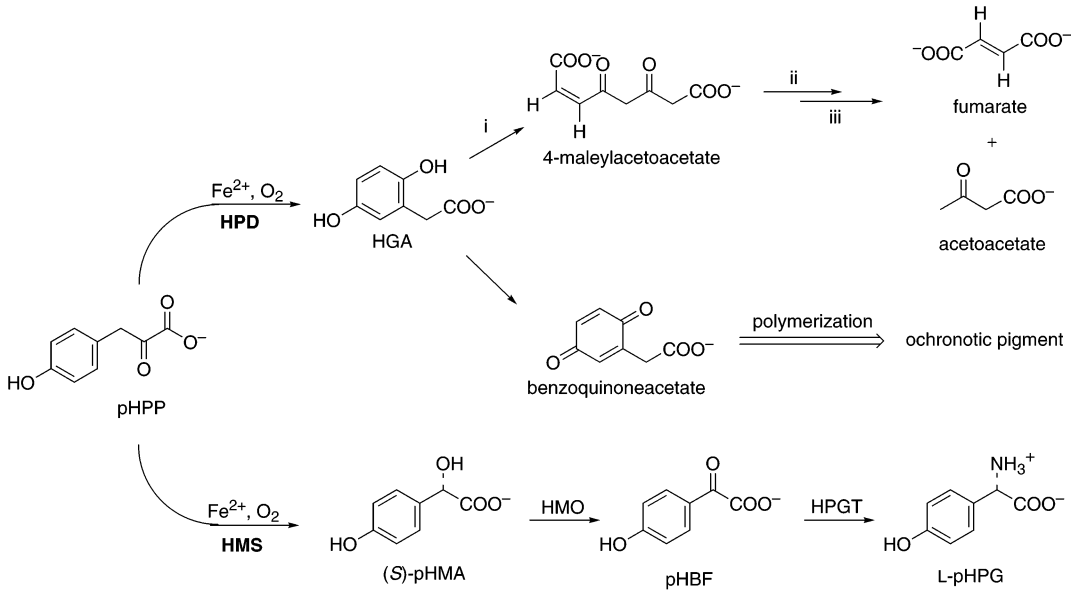

[a] (i) Homogentisate oxidase; (ii) 4-maleylacetoacetate isomerase; and (iii) 4-fumarylacetoacetate lyase.

The Fe^{2+}/oxygen-dependent HPD shows strong primary sequence homology to members of the *p*-hydroxymandelate synthase (HMS) family of enzymes involved in secondary metabolism, specifically, the biosynthesis of *p*-hydroxyphenylglycine (Scheme 1). HMS catalyzes the first step of the biosynthesis of this nonproteinogenic amino acid in which pHPP is decarboxylated and hydroxylated to produce (*S*)-*p*-hydroxymandelate (pHMA), as demonstrated in this laboratory (S. Bantia, M. Gunsior, and C. A. Townsend, unpublished results) and others (*24*, *25*). pHMA is further oxidized to L-*p*-hydroxybenzylformate (pHBF) and transaminated to *p*-hydroxyphenylglycine (pHPG) (*24*). The lower homologue of tyrosine, pHPG, is incorporated into several biologically active secondary metabolites including vancomycin (*26*), complestatin (*27*), the β-lactam antibiotic nocardicin A (*28*), calcium-dependent antibiotic (CDA) (*29*), and ramoplanin (*30*). L-pHPG biosynthetic genes were first identified in *Amycolatopsis orientalis* as part of the cluster responsible for the production of chloroeremomycin, a glycopeptide whose aglycon has the same structure as vancomycin (*31*). Homologues have also been identified in *Streptomyces coelicolor* (*32*), the producer of CDA, *Amycolatopsis mediterranei* (*33*), *Streptomyces lavendulae* (*34*), and *Nocardia uniformis*, the organism that produces nocardicin A (M. Gunsior, S. D. Breazeale, and C. A. Townsend, unpublished results).

The similarities in primary sequence (25−35% identity) and function between these two internal dioxygenases raise an interesting question of catalytic differentiation. Both are Fe^{2+}/O_2-dependent and utilize pHPP as substrate, yet form different products. The initial half-reaction, oxidative decarboxylation, is presumably the same for both enzymes, but the product-determining stage in HPD and HMS must be distinct. It has long been postulated in α-KG/Fe^{2+}-dependent enzymes that the oxygenating intermediate is a reactive Fe(IV)-oxo species. The first direct evidence for this proposed intermediate was recently obtained from taurine/α-KG dioxygenase (*35*).

The recently published crystal structure of *Pseudomonas fluorescens* HPD reveals the amino acid residues lining the active site pocket (*16*). These data, in conjunction with sequence alignments and secondary structure predictions of known HPDs and HMSs, highlight the similarities and differences between the two enzymes. In particular, four residues in HPD enzymes were identified that may play a role in substrate binding, positioning, and directing catalysis. These residues, Pro214, Asn216, Phe337, and Phe341 (numbered according to *P. fluorescens* HPD, P80064), were mutated individually and in combination to the corresponding residues in HMS, Thr, Ile, Ile, and Tyr, respectively, in an effort to convert the *Streptomyces avermitilis* HPD into a novel *S. avermitilis* HMS. Stepwise, rational site-directed mutagenesis led to the isolation of a mutant HPD capable of producing the normal product, HGA, the desired product, pHMA, and a third unexpected compound derived from a reaction intermediate. Site-directed mutagenesis of HPD active site residues provides the first structural evidence for the involvement of an arene−oxide intermediate in the side chain migration previously postulated in HGA biosynthesis.

EXPERIMENTAL PROCEDURES

Materials. Microbiological media were purchased from Difco Laboratories (Detroit, MI). Restriction enzymes were obtained from Strategene (La Jolla, CA) and New England Biolabs (Beverly, MA). *Escherichia coli* BL21 (DE3) expression cells and pET28b+ vector were purchased from Novagen (Madison, WI). Platinum Taq polymerase, PCR4 Topo vector, and *E. coli* TOP10 cells were obtained from Invitrogen (Carlsbad, CA). Econo-Pac 10DG Desalting columns were purchased from Bio-Rad (Hercules, CA). Ni^{2+}-NTA resin and Miniprep Plasmid Purification kits were obtained from Qiagen (Valencia, CA). pHPA, pHMA, HGA, pHPP, ascorbate, Fe(II) ascorbate, bovine liver catalase, and kanamycin were acquired from Sigma-Aldrich (St. Louis, MO). IPTG was purchased from Fisher Scientific (Fairlawn, NJ), T4 DNA ligase was obtained from Roche Diagnostics Corporation (Indianapolis, IN), and synthetic oligonucleotides were prepared by Sigma-Genosys (The Woodlands, TX). Plasmid pCD661 containing wild-type *S. avermitilis* HPD

was a generous gift of Dr. Claudio Denoya (Pfizer, Groton, CT).

General Methods. PCR experiments were performed using a GeneAmp PCR system 2400 (Perkin-Elmer; Norwalk, CT). DNA manipulations (restriction digests, ligation reactions) were performed according to manufacturer's directions. All sequencing was performed using the PRISM Dye Terminator Cycle-Sequencing Ready Reaction kit (ABI, Foster City, CA) and the PE Applied Biosystems 377 Prism DNA Sequencer at the Johns Hopkins School of Medicine Sequencing Facility, Department of Biological Chemistry. Secondary sequence homology comparisons were performed using the PSIPRED Protein Structure Prediction Server (*36*). For phylogenetic analysis, peptide sequences were aligned using ClustalW multiple sequence alignment software (*37*) using the following accession numbers: CAA04693, NP_108430, P23996, 1_CJX, AAK24504, F83537, C82211, O06695, CAC47521, Q55810, AAP07321, CAB51008, Q53586, CAD70479, AAK48714, 042764, NP_058929, NP_002141, AAF51601, Q18347, CAD42488, CAC48371, T17470, CAB38519, AAM80551, and AAK81835. The distance matrixes were calculated from these alignments using the Kimura protein distance algorithm (*38*), and phylogenetic trees were generated using the Neighbor Joining method of Saitou and Nei (*39*) and visualized with TreeView (*40*). Mass spectrometric analyses were performed at the Nebraska Center for Mass Spectrometry (Lincoln, NE).

Molecular Modeling. All molecular modeling was performed on an SGI Octane 2XR10000 workstation using Insight II software (Accelerys, San Diego, CA). The crystal coordinates of *P. fluorescens* HPD were obtained from the Protein Data Bank (http://www.rcsb.org/pdb/; ID: 1CJX**)**. The proposed intermediate *p*-hydroxyphenylacetate (pHPA) was created with Builder Module and minimized using the Discover DVFF force field. pHPA was manually positioned into the active site using Insight II. Four restraints corresponding to iron coordination bonds with His161, His240, Glu322, and the carboxylate of the pHPA molecule were set in the range of 1.8−2.3 Å. The CVFF force field Steepest Descent algorithm (1000 iterations) was used to minimize large steric interactions, followed by the Conjugate Gradients algorithm until the maximum RMS derivative was less than 0.001 kcal/Å. The mutant enzyme was created using HPD docked with pHPA; Phe337 was changed to Ile and minimized as stated previously.

Cloning of Wild-Type and Mutant HPD Proteins. The *S. avermitilis* HPD gene was excised from pCD661 using *Nde*I and *Eco*RI, gel purified, and ligated to the complementary sites of pET28b+. Ligation products were transformed into *E. coli* BL21(DE3) for heterologous expression and sequence analysis. The resulting construct, pET-Sa-HPD, contained an N-terminal His_6 affinity tag. The sequence of the subcloned gene revealed the presence of three additional bases at position 120 not part of the original published sequence, which results in a second tyrosine residue at position 40. The error was also noted in a recent paper regarding substrate addition for *S. avermitilis* HPD (*19*). The single mutant F337I was obtained by PCR amplification of a subfragment of pCD661-HPD using the primers HPD-Nterm*Nde*I-A and Cterm*Eco*NI, where *Eco*NI (Table 1) introduced the desired T → A mutation. The amplified product was gel purified, digested with *Nde*I and *Eco*NI, and ligated into the corresponding cloning sites of pCD661-HPD resulting in plasmid pCD661-F337I, from which pET-F337I plasmid was prepared as described for pET-Sa-HPD.

Table 1: Synthetic Oligonucleotides Used for Site-Directed Mutagenesis[a]

primer name	nucleotide sequence (5′-3′)
HPD-NtermNdeI-A	TATA*CATATG*ACGCAGACCACACACCACAC
HPD-CtermEcoRI-D	AGGGC*GAATTC*GAGCTCGGTACC
CtermEcoNI	ATCG*CCTCGAACAGG*GCCTTGA**T**GTTGCC
P214Trev-B	ATCG**T**GAACTTGACCTTGAGCGTG
P214Tfor-C	CACGCTCAAGGTCAAGTTC**A**CGAT
N216Irev-B	GAGGGCGGGCTCG**A**TGATCG
N216Ifor-C	CGATCA**T**CGAGCCCGCCCTC
F341Yrev-B	CGATCGCCTCG**T**ACAGGGCCTT
F341Yfor-C	AAGGCCCTGT**A**CGAGGCGATCG
pET28-ClaI-R	GCGAT*ATCGAT*TGTATGGGAAGCCC

[a] Restriction sites are indicated in italics, and the introduced mutation is in bold.

The mutant constructs P214T, N216I, F341Y, P214T/N216I, P214T/F337I, N216I/F337I, and P214T/N216I/F337I were generated by PCR amplification using the overlap extension mutagenesis method (*41*) with templates and primers as detailed in Tables 1 and 2. Amplification products were blunt cloned into pCR4-TOPO vector and transformed into *E. coli* TOP10, and mutation identities were confirmed by DNA sequencing. Clones containing the desired mutation-(s) were digested with *Nde*I and *Hin*dIII and ligated into the complementary sites of pET28b+. The mutant constructs containing the F341Y mutation could not be obtained by the overlap extension method due to the proximity of F341Y to both the end of the gene and Phe337. To preserve possible F337I mutations, a method involving restriction digestion and ligation was used. HPD and mutant gene constructs in pET28b+ vector contained two *Bss*HII restriction sites, one located between Asn216 and Phe337 and a second in the *lacI* gene, which, when digested, yields two fragments of 2147 and 4318 bp. The larger fragment contains positions 337 and 341, while the smaller fragment contains residues 214 and 216. In this manner, pET-P214T/F341Y, pET-N216I/F341Y, pET-F337I/F341Y, pET-N216I/F337I/F341Y, and pET-P214T/N216I/F341Y were prepared by ligating combinations of these fragments.

Expression of Wild-Type and Mutant HPD Constructs. Cultures of *E. coli* BL21(DE3) cells (5 mL) containing the recombinant pET28b+ plasmid were prepared by inoculating single colonies from agar plates into 3 mL of LB containing 25 μg/mL kanamycin and incubated overnight at 37 °C with shaking (300 rpm). The saturated cultures were diluted 1:100 in LB containing 25 μg/mL kanamycin and grown at 37 °C with shaking (300 rpm) to an optical density at 600 nm (A_{600}) of 0.6. Expression was induced with the addition of 1 mM IPTG and proceeded 24 h at the above conditions. Cells were harvested by centrifugation (5000*g*, 15 min), resuspended in 4 mL of lysis buffer (50 mM sodium phosphate, pH 8, 300 mM NaCl, 10 mM imidazole), and stored at −20 °C.

Purification of Wild-Type and Mutant HPD Enzymes. Purification was performed from 4 mL of resuspended cell culture. Cultures were subjected to sonication (12 × 10 s bursts with 10 s rests) using a tuned microtip at 40% amplitude. The lysate was centrifuged at 10 000*g* to pellet cell debris, and the supernatant was applied to a 2 mL Ni^{2+}-NTA column. The column was washed with 10−15 mL of

Table 2: Templates and Synthetic Oligonucleotides Used for Site-Directed Mutagenesis

template	primer pairs	product
pCD661/Sa-HPD	HPD-NtermNdeI-A, P214Trev-B; P214Tfor-C, HPD-CtermEcoRI-D	P214T
pCD661/Sa-HPD	HPD-NtermNdeI-A, N216Irev-B; N216Ifor-C, HPD-CtermEcoRI-D	N216I
pCD661-F337I	HPD-NtermNdeI-A, P214Trev-B; P214Tfor-C, HPD-CtermEcoRI-D	P214T/F337I
pCD661-F337I	HPD-NtermNdeI-A, N216Irev-B; N216Ifor-C, HPD-CtermEcoRI-D	N216I/F337I
pET-N216I	HPD-NtermNdeI-A, P214Trev-B; P214Trev-B, HPD-CtermEcoRI-D	P214T/N216I
pET-PT/FI	HPD-NtermNdeI-A, N216Irev-B; N216Ifor-C, HPD-CtermEcoRI-D	P214T/N216I/F337I
pCD661/Sa-HPD	HPD-NtermNdeI-A, F341Yrev-B; F341Yfor-C, HPD-CtermEcoRI-D	F341Y
pET-PT/NI/FI	HPD-NtermNdeI-A, F341Yrev-B; F341Yfor-C, pET28-ClaI−R	P214T/N216I/F337I/F341Y

wash buffer (50 mM sodium phosphate, pH 8, 300 mM NaCl, 20 mM imidazole) followed by a 4 mL elution of elution buffer (50 mM sodium phosphate, pH 8, 300 mM NaCl, 250 mM imidazole). The purified protein was desalted on an Econo-Pac 10DG desalting column equilibrated with assay buffer (50 mM Tris, pH 8, 10% glycerol). A total of 4 mL of assay buffer was used to elute the protein. Homogeneous enzyme was then concentrated to approximately 1 mL using a Collodian apparatus equipped with a 10 000 MWCO membrane against 50 mM Tris, pH 8, 10% glycerol.

Spectroscopy. Circular dichroism measurements were made in 0.2 mm cells in a Jasco J-810 spectropolarimeter operated at a scan rate of 20 nm/min in the range of 190−300 nm. Protein samples were prepared in 10 mM Tris (pH 8.0) at a concentration of 5 μM.

Activity Assay for Wild-Type and Mutant Enzymes. The reaction mixture contained 1−2 μM enzyme, 50 mM Tris, pH 8, 0.25 mM ferrous ion, 0.5 mM ascorbate, 0.1 mg/mL bovine liver catalase, and 1 mM substrate, pHPP. The reaction was started by the addition of substrate and allowed to proceed for a fixed time at room temperature. Following the addition of acetonitrile (15% final concentration) to stop the reaction, the solution was centrifuged for 20 min at 16 000*g*.

Products were analyzed by HPLC on a Luna C18 (5 μm) analytical column (250 × 4.6 mm; Phenomenex, Torrance, CA) at a flow rate of 1 mL/min. The solvents used were ddH_2O/0.01% TFA (A) and acetonitrile/0.01% TFA (B). A total of 100 μL of each reaction was analyzed under the following gradient conditions: 5 min 100% A/0% B, 20 min linear gradient from 100% A/0% B to 80% A/20% B, 5 min 80% A/20% B, and 10 min 100% A/0% B. The elution of components was monitored at 220 nm.

Isolation of Oxepinone. The standard reaction assay using the P214T mutant was scaled up 40× and incubated overnight at room temperature. Following the addition of acetonitrile to stop the reaction, the solution was filtered through a 0.22 μm filter. HPLC separation was carried out on a Luna C18 (5 μm) semipreparative column (250 × 10 mm; Phenomenex) at a flow rate of 5 mL/min using the same gradient as detailed above. Fractions containing the unknown coproduct (t_r 18 min) were collected, concentrated under vacuum to remove acetonitrile, and lyophilized to afford a tan powder. MS *m*/*z* 169.1 $(M + H)^+$, exact mass 169.049 (calcd $M + H^+$ 169.050, $C_8H_9O_4$); MS/MS $(M + H)^+$ 123.0, 109.0, 67.0. ^{1}H NMR (D_2O, 0.1% DCl) δ 7.15 (d, $J = 10.4$ Hz, 1H), 6.95 (dd, $J = 10.4$, 0.8 Hz, 1H), 6.26 (d, $J = 10.4$ Hz, 1H), 6.21 (d, $J = 10.4$ Hz, 1H), 5.04 (ddd, $J = 6.0$, 5.2, 0.8 Hz, 1H), 3.03 (dd, $J = 17.2$, 5.2 Hz, 1H), and 2.97 (dd, $J = 17.2$, 6.0 Hz, 1H).

RESULTS

Phylogenetic analysis was performed on the HPD/HMS family of dioxygenases (Figure 1). The HPD protein family clusters in three groups: the eukaryotes, Gram-negative (including cyanobacteria) and Gram-positive eubacteria. Interestingly, the Gram-positive eubacteria clade is composed of only three members, all of which are soil microorganisms. Because other Gram-positive eubacteria do not contain this enzyme, HPD activity likely reflects the metabolic adaptation of both the *Bacillus cereus* group of organisms and the streptomycetes. HPD dioxygenases appear to be more common in Gram-negative eubacteria, as exemplified by the larger number of HPD sequences derived from genome sequencing projects. In addition, Figure 1 shows that Gram-positive HPDs are more closely related to those of eukaryotic origin than to other eubacterial HPDs. The HMS family of dioxygenases has a relatively higher sequence identity (ca. 31%) with the Gram-positive eubacterial HPDs than either the eukaryotic (ca. 26%) or other eubacterial HPDs (ca. 23%). For this reason, we chose to engineer the *S. avermitilis* HPD into a novel *S. avermitilis* HMS.

Elucidation of a *P. fluorescens* HPD crystal structure yielded insight into the residues lining the active site. Residue conservation is not evenly distributed throughout the protein (Figure 2). Most of the conserved residues are found in the C-terminal domain of HPD, which contains the catalytic iron essential for activity (*16*, *42*). The smaller N-terminal domain shows much lower homology and is not reported to have any catalytic function, but mutations in this region can affect activity. For example, patients suffering from Hawkinsinurea possess an A33T mutation in HPD (*2*).

A common structural motif among non-heme-Fe^{2+}/O_2 dependent enzymes is a 2-His-1-carboxylate facial triad in which two histidines and one aspartate/glutamate ligand occupy one face of the iron (II) coordination sphere (*43*). Members of the α-KG-dependent dioxygenase family can be further grouped based on the spacings among these three

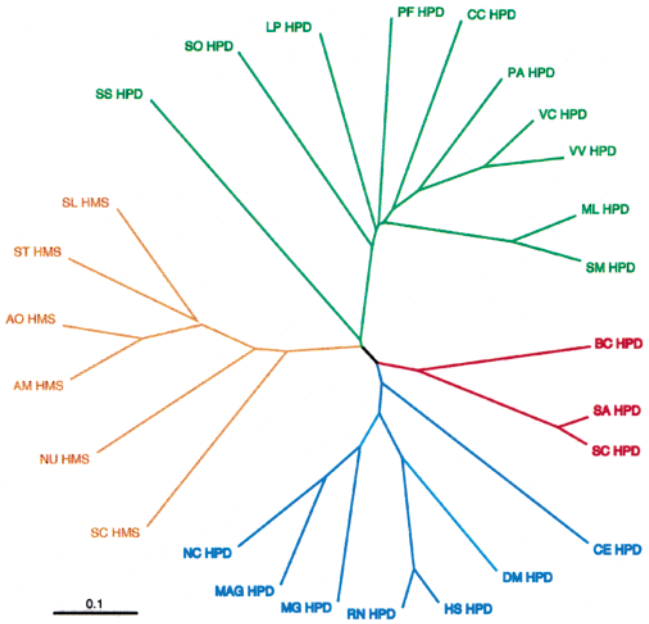

FIGURE 1: Phylogenetic tree illustrating the evolutionary relationship between HPDs of various origin. The green clade represents HPD of Gram-negative eubacterial origin, while those in red and blue are from Gram-positive eubacteria and eukaryotic organisms, respectively. HMS enzymes cluster in a distinct orange clade. Abbreviations are as followed: LP, *Legionella pneumophila*; ML, *Mesorhizobium loti*; SO, *Schewalenella oneidensis*; PF, *Pseudomonas fluorescens*; CC, *Caulobacter crescentus*; PA, *Pseudomonas aeruginosa*; VC, *Vibrio cholerae*; VV, *Vibrio vulnificus*; SM, *Sinorhizobium meloti*; SS, *Synechosystis* sp. PCC6803; BC, *Bacillus cereus*; SC, *Streptomyces coelicolor*; SA, *Streptomyces avermitilis*; NC, *Neurospora crassa*; MAG, *Magnaporthe grisea*; MG, *Mycosphaerella graminicola*; RN, *Rattus norvegicus*; HS, *Homo sapiens*; DM, *Drosophila melanogaster*; CE, *Caenorhabditis elegans*; NU, *Nocardia uniformis*; AM, *Amycolatopsis mediterranei*; AO, *Amycolatopsis orientalis*; ST, *Streptomyces toyocaensis*; and SL, *Streptomyces lavendulae*.

ligands. Group I enzymes possess the motif $HXDX_{50-70}H$ and consists of enzymes such as isopenicillin N-synthase (IPNS) and deacetoxycephalosporin C-synthase (DAOCS), group II $[HX(D/E)X_{138-207}H]$ includes the enzyme clavaminate synthase, and group III members such as proline hydroxylase exhibit the motif $HXDX_{72-101}H$ (*44*). In contrast to other α-KG-dependent enzymes, however, HPD and HMS enzymes do not fall into any of the previous three categories, possibly because the α-keto reaction partner is internal rather than external to the substrate.

The crystal structure of *P. fluorescens* HPD revealed the residues involved in Fe(II) coordination: His161, His240, and Glu322, all of which are conserved among known HMS and HPD enzymes (data not shown). These data also serve as a basis for comparison of secondary structure predictions. The predicted structural elements of *N. uniformis* HMS and *S. avermitilis* HPD are highly similar to the observed structure of *P. fluorescens* HPD, as shown in Figure 2, and suggest that the HMS and HPD enzymes possess the same overall fold in vivo. Comparison of the two types of enzyme and the crystal structure data show distinct differences in the residues lining the active site. Seven residues are universally conserved in both families (Leu307, Gln309, Phe311, Phe332, Gly333, Asn336, and Leu340). Other invariant residues (Asp160, Gln239, and Arg326) are involved in hydrogen bonding interactions to iron-coordinating ligands. Of the remaining residues in the active site, five are conserved among HPD enzymes but distinct in HMS. Specifically, Leu199, Pro214, Asn216, Phe337, and Phe341 in HPDs have become Met, Thr, Ile, Ile, and Tyr, respectively, in the HMS active site. These residues appear to be the determining factor in a priori classification of HMS or HPD activity. Active site modeling of the HPD enzyme indicated that Leu199 would have minimal interaction with substrate and thus was not chosen for mutation.

Generation and Purification of Recombinant Mutant Enzymes. A set of 16 mutants was constructed by PCR amplification from the wild-type enzyme *S. avermitilis* HPD. The mutations P214T, N216I, F337I, and F341Y were prepared individually and in combination. All mutants were expressed as *N*-terminal His_6-tagged fusions in the heterologous host *E. coli* BL21(DE3). Each culture was incubated for 24 h in the presence of IPTG to allow pigmentation to develop; under alkaline and aerobic conditions, HGA oxidizes and polymerizes to form an ochronotic pigment. This pigment is dark brown and clearly discernible in growing cultures. The intensity of the ochronotic pigment is proportional to HGA production, with wild-type HPD giving the darkest hue. F341Y, F337I, P214T, and N216I recombinant mutants all produced pigmentation and are listed in order of decreasing color intensity. The mutants were purified to homogeneity by Ni^{2+}-affinity column chromatography as determined by SDS−PAGE. A representative purification as well as the purified single mutants are shown in Figure 3A,B.

Biochemical Analysis of Catalytic Activity. HPD activity in other systems is greatly affected by additives such as catalase and ascorbate (*15*), complicating comparisons to recent studies (*19*). Additionally, spontaneous decarboxylation of substrate can occur in the presence of such stimulators (*1*). pHPP exists in both enol and keto tautomeric forms, of which the enol form has been shown to have an inhibitory effect on HPD from *Pseudomonas* sp. P. J. 874 (*45*). The enol form predominates in ethanol solutions but quickly equilibrates to approximately 97% keto tautomer under aqueous conditions (*17*). To best assay the effect of each mutation on wild-type activity, the change in HGA production was monitored under a fixed-time assay and a given set of conditions and then compared to the wild-type activity (Table 3). Negative controls with heat-inactivated enzyme ensured the conditions did not cause a spontaneous decarboxylation of pHPP. Ascorbate, bovine liver catalase, and exogenous Fe^{2+} were experimentally determined to be necessary for optimal activity, as well as the addition of substrate to start the reaction. The same activating effect of the additives was noted in HPD from a *Pseudomonas* species (*15*). Preliminary analysis of the wild-type and mutant HPD catalytic behavior indicated substrate inhibition, in accordance with recent studies of the enzyme from *S. avermitilis* (*19*) and other organisms (*1*, *15*).

As expected, wild-type HPD produced HGA without the formation of side products. In older HPD enzyme preparations, however, a small peak at approximately 22 min was observed, which possessed the same retention time and UV spectrum as pHPA. This peak, absent in the negative control, was shown to coelute with an authentic sample of pHPA (data not shown). Uncoupling of the reaction, or formation of CO_2 without hydroxylation, is known to occur in α-KG-

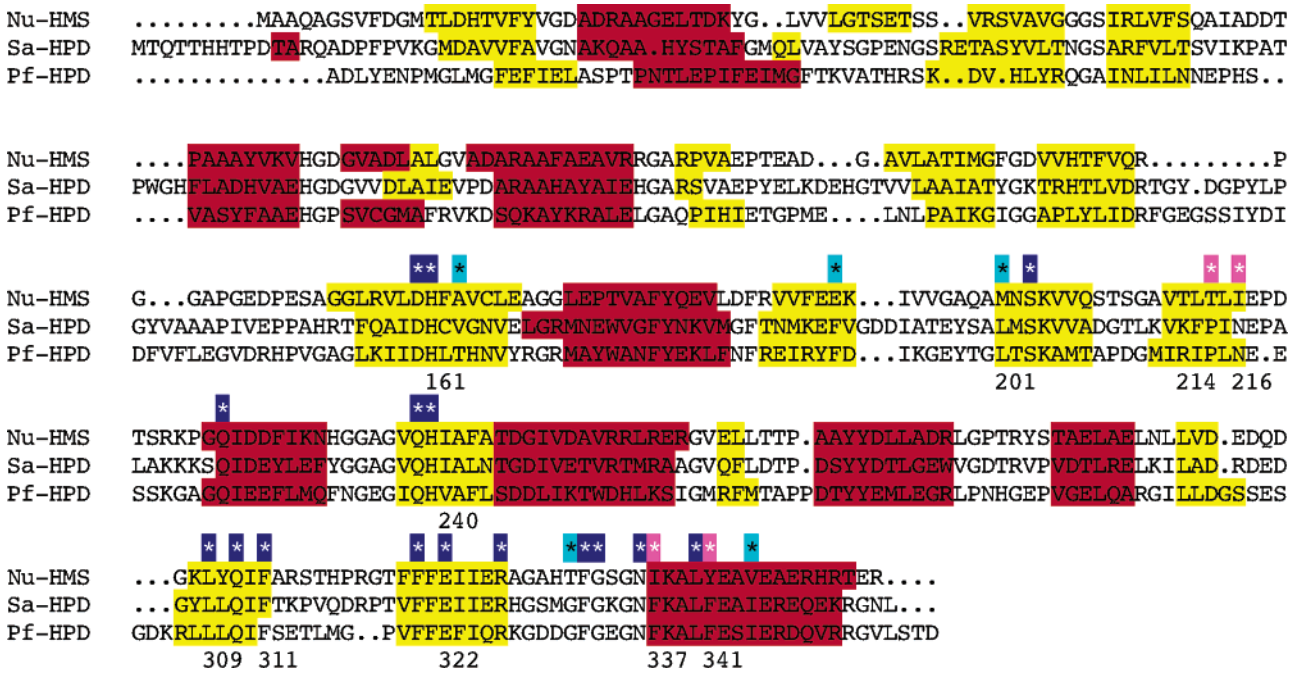

FIGURE 2: Secondary structure alignment of HPD and HMS enzymes. Nu: *N. uniformis*, Sa: *S. avermitilis*, and Pf: *Pseudomonas fluorescens*. The residues highlighted in red are helical in structure, while those in yellow represent β-sheets. Blue-asterisked residues are conserved between the HMS and HPD enzymes; those denoted by a pink asterisk are conserved among each separate family and were chosen for mutation. The residues in pale blue are different in the HMS family but distant from the active site.

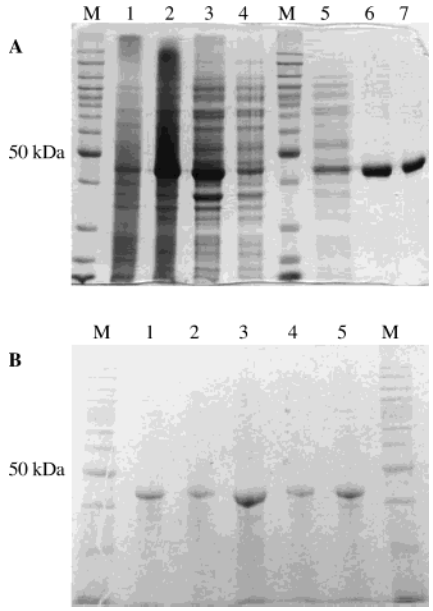

FIGURE 3: (A) SDS−PAGE gel analysis of a representative purification of HPD and mutants. M: Invitrogen benchmark protein ladder; 1, uninduced sample; 2, induced sample; 3, cell free extract; 4, flow-through; M; 5, wash; 6, elute; and 7, desalt fractions. (B) Purified single mutants. M; 1, wild-type HPD; 2, P214T; 3, N216I; 4, F337I; and 5, F341Y.

dependent enzymes (*46*−*48*). The following mutants were inactive, even after incubations greater than 12 h: P214T/N216I, N216I/F337I, N216I/F341Y, P214T/N216I/F337I, P214T/N216I/F341Y, P214T/F337I/F341Y, N216I/F337I/F341Y, and the quadruple mutant P214T/N216I/F337I/F341Y.

The remaining mutants (P214T/F337I, P214T/F341Y, and F337I/F341Y) produced small amounts of one or both of the two postulated products, HGA and pHMA, or a third unexpected unknown compound. Characterization of the unknown compound, described below, revealed it to be an oxepinone (inset, Scheme 3). While mutants with three or four amino acid changes were inactive, those with two mutations did support product formation to a small extent, if at all, as demonstrated by the low but detectable production of ochronotic pigment (data not shown). Figure 4 illustrates the product-forming behavior of selected mutants. The quadruple mutant, for which no activity was observed, serves as a negative control. N216I was the least active of the single mutations with activity 667-fold less than wild-type HPD. The largest amount of HGA (denoted by a white arrow in Figure 4) was produced by F341Y, in addition to a small amount of the oxepinone. Significant amounts of both HGA and oxepinone (gray arrow, Figure 4) were formed by P214T and F337I. None of the mutants achieved the desired goal of completely converting HPD product formation from HGA to pHMA, although both P214T and F337I catalyzed formation of pHMA (black arrow, Figure 4) in addition to HGA, as well as the unexpected oxepinone compound. Comparison of the wild-type enzyme, each single mutant, and the quadruple mutant by CD spectroscopy revealed no significant conformation changes among the proteins as shown in Figure 5.

Table 3: Relative Activities of HPD Mutants with Respect to HGA Formation

enzyme	rel. act. (%)
wild-type	100
P214T	1.6
N216I	0.15
F337I	0.67
F341Y	16.9

Structure Determination of the Oxepinone. A larger scale incubation of the P214T mutant was undertaken, and the unknown coproduct was isolated by preparative reverse-

Scheme 2

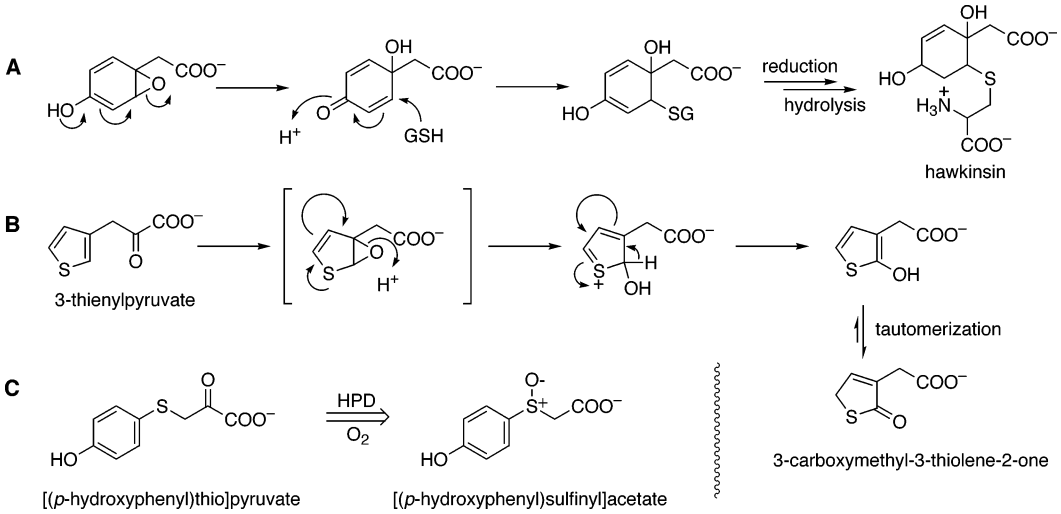

Scheme 3: Proposed Mechanism of HGA and Oxepinone Formation[a]

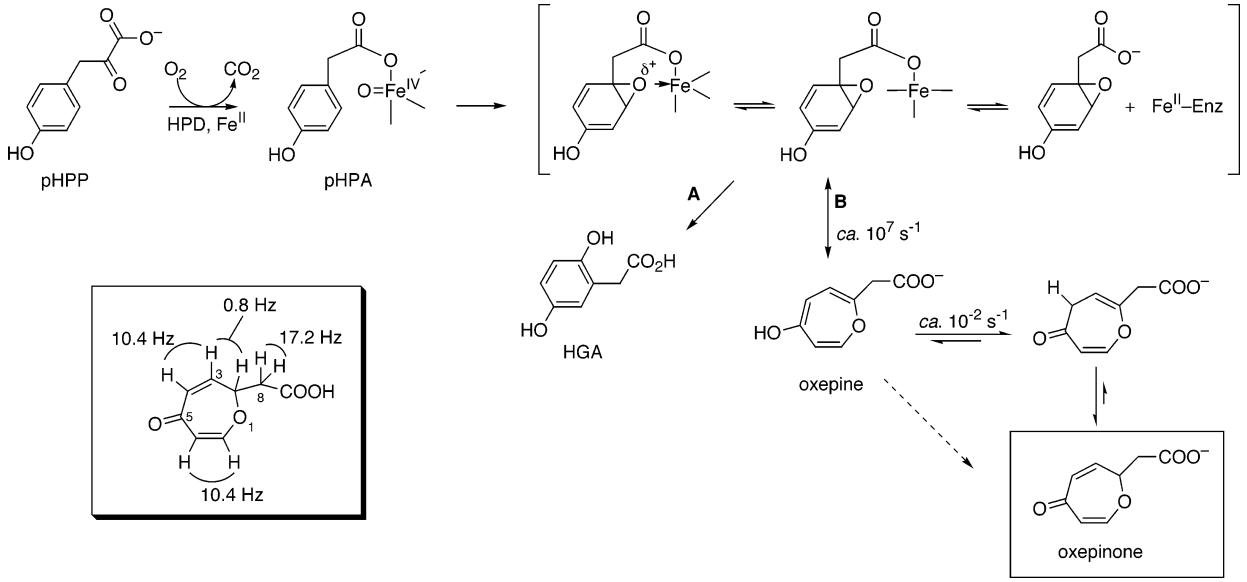

[a] Inset: coupling constants of oxepinone structure.

phase HPLC. A ^{1}H NMR spectrum was recorded in D_2O. Immediately striking were two pairs of doublets at low field indicative of an olefinic rather than aromatic product, and the AB part of an apparent ABX pattern was visible at a higher field. The vicinal coupling constant of all four alkene hydrogens was 10.4 Hz, a large value consistent with their presence in a seven-membered ring. One alkene doublet at δ 6.95 was further split by a 0.8 Hz coupling. Homonuclear decoupling of this resonance caused the alkene doublet at δ 6.21 to collapse to a singlet and simplified a multiplet at δ 5.04. The latter signal was assigned to H-2 (inset, Scheme 3) in the oxepinone, and the decoupling experiment allowed H-3 and H-4 to be assigned as well. As expected, irradiation of H-7 at δ 7.15 caused its coupling partner H-6 at δ 6.26 to reduce to a singlet. Finally, irradiation of the H-2 methine simplified the upfield AB pattern establishing it as the X of the ABX spin system. The geminal coupling constant of 17.2 Hz measured between the diastereotopic AB hydrogens at C-8 was consistent with a directly attached carboxylate in keeping with comparisons to models and the deduced structure of the oxepinone (inset, Scheme 3). On the basis of the observation of two isolated alkene spin systems, apart from a contiguous ABX system, the oxepinone structure shown in Scheme 3 was readily advanced for the unknown compound. This assignment was further substantiated by an exact mass determination and MS/MS fragmentation of the parent ion to yield cleavage products in keeping with loss of water and carbon monoxide and of the acetyl side chain.

Modeling. The crystal structure of HPD shows homology to the extradiol dioxygenase family (*16*) whose members are not α-KG-dependent, nor do they require ascorbate for maximal activity. Circular dichroism and crystal studies of α-ketoacid-dependent dioxygenases (*49*−*51*) indicate that α-KG binds to the six-coordinate ferrous center in a bidentate manner during the first stage of the catalytic mechanism. Binding of substrate results in a shift from six- to five-coordinate geometry at the active site in preparation for oxygen binding (*51*, *52*). The first stage of binding is believed to be identical in the catalytic mechanisms of internal dioxygenases HPD and HMS, except that the α-ketoacid cofactor is part of the substrate itself. This unusual circumstance may account for the observation that *P. fluorescens*

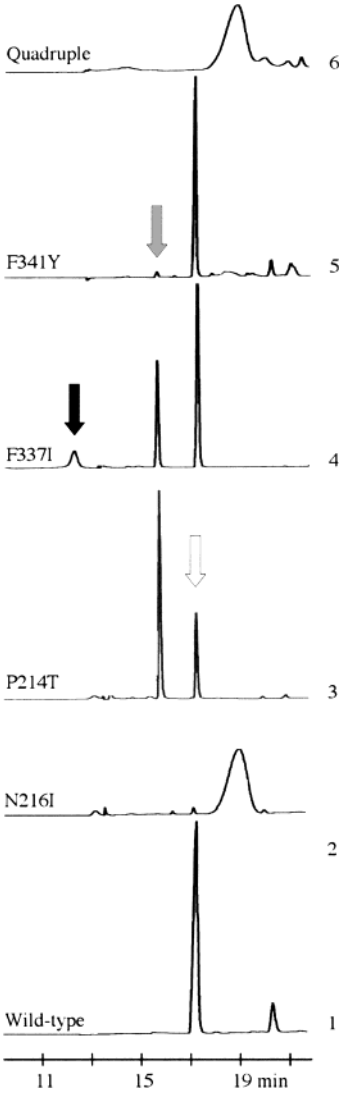

FIGURE 4: HPLC chromatograms illustrating the product forming behavior of HPD and mutants. 1: HPD, 2: N216I, 3: P214T, 4: F337I, 5: F341Y, and 6: quadruple mutant. White arrow, HGA; gray arrow, oxepinone; and black arrow, pHMA.

HPD possesses an uncommon distorted tetrahedral geometry about Fe in the absence of substrate (*16*).

Further studies of HPD enzymes have shown a bi−bi mechanism in which substrate pHPP is the first to bind and CO_2 is the first product to dissociate (*19*, *53*). Circular dichroism studies of *S. avermitilis* HPD revealed a weak ligand charge-transfer band at 500 nm indicative of bidentate substrate binding in accord with the behavior of α-KG dependent oxygenases (*19*). In the next step, oxygen binding and decarboxylation are proposed to occur to form a reactive iron−oxo intermediate analogous to that recently characterized for the first time with taurine dioxygenase (*35*). Decarboxylation of pHPP results in *p*-hydroxyphenylacetate (pHPA), believed to be bound to the active site Fe in a monodentate manner, analogous to studies done on other Fe^{2+}/α-KG-dependent dioxygenases, in which decarboxylation of α-KG results in monodentate binding of succinate (*54*). For the cases of HPD and HMS, we propose that the respective active sites govern the reaction of this potent oxidant to partition between the two products to give either arene oxidation or hydroxylation at the reactive benzylic locus.

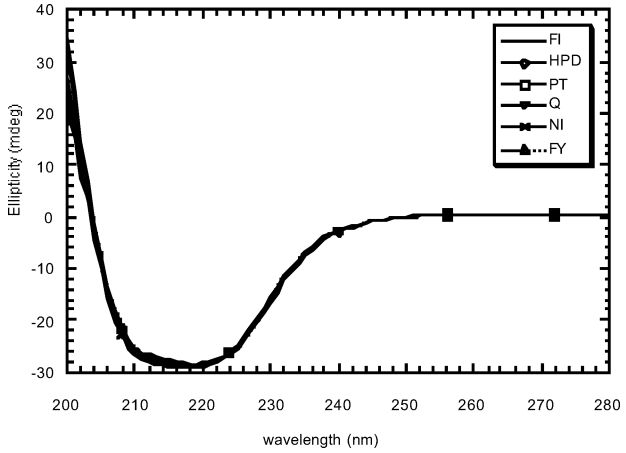

FIGURE 5: CD spectra of the wild-type HPD, single mutants P214T, N216I, F337I, F341Y, and the quadruple mutant. Each sample was scanned three times from 190 to 300 nm.

The postulated pHPA intermediate minimized within the active site of the wild-type enzyme showed π-stacking interactions with Phe337, in addition to a hydrogen bond between the terminal phenol and Asn216. In contrast, the single amino acid replacement F337I slightly reduces the steric bulk of this residue and removes the possibility of $\pi-\pi$ interaction. As a consequence, the aryl ring of the substrate rotates toward the site of mutation and twists to change the orientation of both the *p*-hydroxyphenyl ring and the benzylic methylene hydrogens of pHMA to the iron site, as shown in Figure 6. While productivity of the mutant enzyme drops about 150-fold from that of wild-type, oxepinone and low levels of pHMA are produced in addition to HGA.

DISCUSSION

The highly similar enzymes HPD and HMS provide a unique opportunity to study the residues in an enzyme active site that mediate catalytic differentiation from a common intermediate during product formation. Both enzymes couple the oxidative decarboxylation of the pHPP keto-acid side chain to presumably the same reactive iron−oxygen species and complexed pHPA but partition and restrict chemistry to the formation of one of two distinct products. Initial decarboxylation of pHPP leads to the proposed *p*-hydroxyphenylacetate/iron−oxygen active site complex. Formation of pHPA by wild-type HPD in an apparent uncoupling of the reaction strongly supports the intermediacy of this reaction partner. HPD goes on to produce HGA through a postulated arene−oxide intermediate, while HMS is thought to carry out a conventional hydrogen abstraction and hydroxylation at the benzylic carbon. Sequence alignments and secondary structure comparisons suggest a well-conserved topology and similar active site binding pockets leading to the question of which residues are involved in directing product formation.

Publication of a high-resolution crystal structure of a bacterial HPD provided insight into the active site architecture, confirming the identification of possible residues that guide reaction to either of the two products. Four residues that uniquely map to either HPD or HMS activity dictated the specific changes to be made. Other residues in the active site were conserved across both enzyme families. Thus, P214T, N216I, F337I, and F341Y were prepared singly and

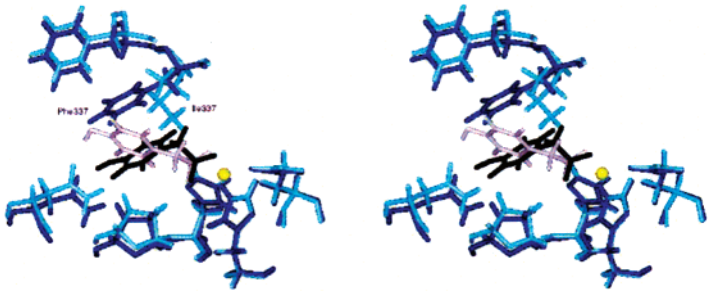

FIGURE 6: Stereoview of the superimposed wild-type HPD and F337I mutant active sites with modeled pHPA intermediate. Dark blue structures and the black intermediate correspond to wild-type enzyme, while light blue structures and the gray intermediate represent the F337I mutant. The catalytic iron atom is yellow.

in combination, and the product profiles were analyzed by HPLC.

Spectroscopic analyses were performed on the wild-type enzyme and selected mutants to ensure that the mutated residues did not adversely affect folding. CD spectra of the single and quadruple mutants were highly similar to that of wild type. As the quadruple mutant retains the wild-type fold, the same was expected for the double and triple mutants. Therefore, the changes in catalytic activity observed in the mutants are believed to result from alterations in the active site and interactions with substrate rather than misfolding. Of the 16 HPD mutants, double mutations showed only slight activity that could not be usefully measured under the assay conditions employed. Triple mutations and the quadruple mutant were devoid of any detectable activity suggestive of diminished binding capacity for substrate. Those mutants bearing only one amino acid substitution, however, retained considerable catalytic activity. The most active of these, F341Y, possessed approximately 17% of wild-type activity relative to HGA formation and produced a small amount of the new oxepinone product. This result is consistent with the position of this residue within the active site somewhat distant from substrate. Mutants P214T and F337I were both moderately active in addition to producing the unexpected oxepinone product and low amounts of pHMA. Of these two mutants, F337I was chosen for molecular modeling based on the presumption that substitution of the Phe would distort the structure less and afford a more accurate view of the mutant protein and its interaction with pHPA. Minimizations of the wild-type enzyme harboring the substrate/iron complex reveals a π-stacking arrangement between substrate and Phe377, while a F337I mutation at this position eliminates the $\pi-\pi$ interaction resulting in displacement of the aryl ring toward the site of mutation and rotation of it and the benzylic methylene relative to the iron center, as shown in Figure 6.

Notably, in both the wild-type and F337I minimized structures, a hydrogen bond between the phenol and Asn216 is evident signifying movement of the side chain of this active site residue to maintain interaction and some degree of substrate orientation in the active site. Removal of this interaction in the N216I mutant yielded the least active single-site mutant, N216I, giving a 667-fold decrease in HGA production. The interaction of Pro214 with substrate and the effect of the P214T mutation are less easily interpreted. The P214T mutant had a 60-fold loss in HGA production, while producing the oxepinone, and a small amount of pHMA.

Additionally, a double mutation, R318C/F337I, was devoid of activity. This mutant possessed an accidental mutation, R318C, located approximately 15 Å from the active site. *P. fluorescens* does not contain this residue, nor do any other members of the Gram-negative eubacterial HPD clade (green, Figure 1). However, among the remaining dioxygenases and synthases, including the *S. coelicolor* and *S. avermitilis* enzymes, an arginine or lysine occurs at this position. R318C/F337I was obtained in pure form and did not support the formation of HGA, while F337I alone did. R318C, an outer-sphere mutation, thus has a large effect on activity of the wild-type enzyme. The absence of this residue from *P. fluorescens*, and hence in the crystal structure, precludes analysis of interaction strictly with residues close to the active site. However, the conservation of arginine across other orthologs and the loss of activity in *S. avermitilis* HPD suggests it to be important.

None of the directed mutations singly abolished activity implying that they do not participate directly in catalysis, or significantly affect iron coordination, but instead serve an important function in the positioning and likely stabilization of the substrate for oxidation at the iron center. The initial intent to create an engineered HPD enzyme capable of producing pHMA was partially successful and yielded the unexpected observation of an oxepine derived shunt product.

HPD from a variety of organisms has been studied for nearly 50 years, yet its mechanism of action has been disputed for much of that time. Hydroperoxidation of the aromatic ring followed by rearrangement has been proposed (*55*), as well as formation of the peracid of pHPA (*56*). Synthesis of the latter failed to give HGA, and fundamental consideration of the chemistry led more recently to hypothesis of a metalated ketyl (*57*). The possible intermediacy of an arene oxide, which would be prone to undergo rearrangement and side chain migration in a classic example of the NIH shift, underlies many of these proposals. Notwithstanding, evidence to support the existence of this pivotal intermediate is indirect. For example, patients suffering from the disease Hawkinsinurea excrete the cysteine adduct hawkinsin (*58*). This disorder is attributed to a defect in HPD (*2*), and the formation of this metabolite has been rationalized by the opening of the hypothetical epoxide intermediate to the electrophilic dienone shown in Scheme 2A. Glutathione (GSH) is present in relatively high concentrations in human cells (*59*) and could readily scavenge this reactive species to give a stable addition product, which upon reduction and proteolysis can be visualized to afford hawkinsin (*60*). Similarly, 3-thienylpyruvate is both a substrate and a mechanism-based inactivator of HPD. A single product is formed, 3-carboxymethyl-3-thiolene-2-one, which has been

Scheme 4: Ketonization Products of Conjugated Systems[a]

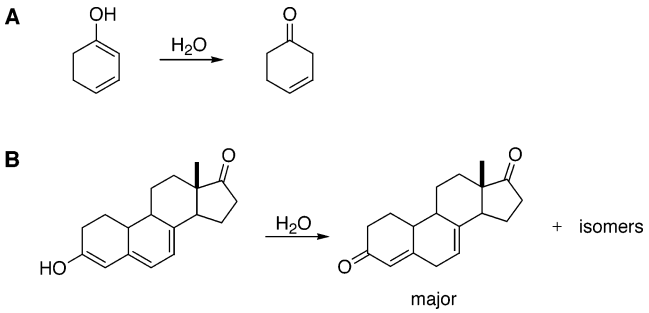

[a] A: Ketonization of a 1,3-cyclohexadienol. B: Ketonization of 3-hydroxy-3,5,7-estratriene-17-one.

proposed to arise by epoxidation of the thiophene ring and rearrangement as depicted in Scheme 2B to give the product (*60*). Finally, and of particular significance to the evolution of HPD to HMS, Pascal showed that when HPD from *Pseudomonas* sp. was presented with [(*p*-hydroxyphenyl)-thio]pyruvate, oxidative decarboxylation took place in the presence of molecular oxygen to give [(*p*-hydroxyphenyl)-sulfinyl]acetate (Scheme 2C) (*61*). Whether the sulfoxide is formed stereospecifically was not determined.

In view of the evident similarity of HPD proteins to the broader class of α-KG-dependent oxygenases (*54*, *62*), current mechanistic thinking favors oxidative decarboxylation of pHPP to a complex of pHPA and a highly reactive iron−oxo species (*18*, *19*). The partitioning of this complex in HPD and HMS to ring epoxidation or benzylic hydroxylation, respectively, as illustrated in Scheme 3, is supported by the findings described in this paper. In particular, for the first time, the existence of the long-postulated benzene oxide intermediate is revealed by its valence isomerization to an oxepine and tautomerization/isomerization to the more thermodynamically stable oxepinone. Kinetic studies of the benzene oxide−oxepine valence isomerization have been hindered by a bias in the equilibrium toward one species or the other. For several aryl substitution patterns where the equilibrium constant is near unity, however, the activation parameters of isomerization have been determined and found to cluster in the range $\Delta G^{\ddagger} = 7-8$ kcal/mol (*63*, *64*). This barrier is quite low, and by application of the Eyring equation (*65*), the rate of unimolecular interchange between arene oxide and oxepine can be estimated as ca. 10^7 s^{-1}. The k_{cat} for HPD from *S. avermitilis* has been determined to be 7 s^{-1} (*19*), vastly slower than this thermally allowed, disrotatory electrocyclization. Why is it that no oxepine-derived products have ever been observed from the wild-type HPD enzymes? The reason for this is the critical difference in the rate of ketonization of a simple enol versus a dienol or a trienol. Tautomerization of the former is orders of magnitude faster than an enol stabilized by conjugation (*66*). For example, the rate of ketonization of 1,3-cyclohexadienol or 3-hydroxy-3,5,7-estratriene-17-one (Scheme 4) in aqueous solution are both approximately 10^{-2} s^{-1} (*66*, *67*). Significantly, the site of protonation in the dienol is exclusively at the α-carbon (*66*), whereas in the trienol at pH 7, the major locus of protonation is the γ-carbon (*67*). The oxepine valence isomer formed in the HPD reaction is a trienol and we illustrate, but cannot prove, its ketonization behavior as a dienol, followed by further isomerization to the more stable, cross-conjugated oxepinone (Scheme 3). Alternatively, protonation could occur at the γ-carbon and give this product directly. The estimated rate of initial ketonization of 10^{-2} s^{-1} in aqueous solution could be further slowed by enol-stabilizing interactions in the enzyme active site. Taken together, k_{cat} for HPD is at least 10^3 times faster than tautomerization/isomerization to oxepine-derived products. We interpret the appearance of the oxepinone among the products of the single-site mutants as a partial release of the arene oxide/oxepine into solution and its subsequent descent to the energetically favorable oxepinone.

It could be argued that the barrier to the interconversion of the enzyme bound benzene oxide to the oxepine would be raised owing to steric compression in the active site hindering seven-membered ring formation. However, given the 10^6-fold higher rate of this process in solution as compared to the turnover of the enzyme, it seems unlikely that the rate of electrocyclization would cease to be competitive with HGA formation. More complex oxidative rearrangement mechanisms than proposed in Scheme 3 could also take place involving, for example, diol formation (*68*). On the other hand, these would entail additional steps in the formation of the benzene oxide required for the appearance of the oxepinone.

The recent kinetic analysis of HPD from *S. avermitilis*, in keeping with the earlier determination of an ordered, bi−bi steady-state mechanism (*53*), demonstrates a second-order reaction of the holo-enzyme in complex with pHPP upon the introduction of oxygen. An intermediate is formed whose first-order decay to product occurs at the catalytically relevant rate of 7.8 s^{-1}. On the basis of the findings we have described, we believe this intermediate is the transiently formed arene oxide/oxepine or an oxygenated species coordinated to the active site iron (Scheme 3) in preference to pHPA. The question of how HPD catalyzes the efficient rearrangement of the benzene oxide intermediate to HGA against the thermodynamic trap of oxepinone formation remains to be answered.

ACKNOWLEDGMENT

We thank Dr. Claudio Denoya for generously providing plasmid pCD661 containing wild-type *S. avermitilis* HPD, Dr. John P. Maxwell and Anthony Stapon for NMR analyses, Dr. Jill M. McFadden for help with the modeling studies, and Dr. Barbara Gerratana for advice on the enzyme analyses.

REFERENCES

1. Lindblad, B., Lindstedt, G., Lindstedt, S., and Rundgren, M. (1977) Purification and some properties of human 4-hydroxyphenylpyruvate dioxygenase (I), *J. Biol. Chem. 252*, 5073−5084.
2. Tomoeda, K., Awata, H., Matsuura, T., Matsuda, I., Ploechl, E., Milovac, T., Boneh, A., Scott, C. R., Danks, D. M., and Endo, F. (2000) Mutations in the 4-hydroxyphenylpyruvic acid dioxygenase gene are responsible for tyrosinemia type III and hawkinsinuria, *Mol. Genet. Metab. 71*, 506−510.
3. Norris, S. R., Shen, X., and DellaPenna, D. (1998) Complementation of the *Arabidopsis* pds1 mutation with the gene encoding *p*-hydroxyphenylpyruvate dioxygenase, *Plant Physiol. 117*, 1317−1323.
4. Schulz, A., Ort, O., Beyer, P., and Kleinig, H. (1993) SC-0051, a 2-benzoyl-cyclohexane-1,3-dione bleaching herbicide, is a potent inhibitor of the enzyme *p*-hydroxyphenylpyruvate dioxygenase, *FEBS Lett. 318*, 162−166.

5. Wu, C. S., Huang, J. L., Sun, Y. S., and Yang, D. Y. (2002) Mode of action of 4-hydroxyphenylpyruvate dioxygenase inhibition by triketone-type inhibitors, *J. Med. Chem. 45*, 2222−2228.
6. Lindstedt, S., Holme, E., Lock, E. A., Hjalmarson, O., and Strandvik, B. (1992) Treatment of hereditary tyrosinaemia type I by inhibition of 4-hydroxyphenylpyruvate dioxygenase, *Lancet 340*, 813−817.
7. Gershwin, M. E., Coppel, R. L., Bearer, E., Peterson, M. G., Sturgess, A., and Mackay, I. R. (1987) Molecular cloning of the liver-specific rat F antigen, *J. Immunol. 139*, 3828−3833.
8. Ruetschi, U., Dellsen, A., Sahlin, P., Stenman, G., Rymo, L., and Lindstedt, S. (1993) Human 4-hydroxyphenylpyruvate dioxygenase. Primary structure and chromosomal localization of the gene, *Eur. J. Biochem. 213*, 1081−1089.
9. Endo, F., Awata, H., Tanoue, A., Ishiguro, M., Eda, Y., Titani, K., and Matsuda, I. (1992) Primary structure deduced from complementary DNA sequence and expression in cultured cells of mammalian 4-hydroxyphenylpyruvic acid dioxygenase. Evidence that the enzyme is a homodimer of identical subunits homologous to rat liver-specific alloantigen F, *J. Biol. Chem. 267*, 24235−24240.
10. Bartley, G. E., Maxwell, C. A., Hanna, W. S., Wittenbach, V. A., and Scolnik, P. A. (1997) Cloning and biochemical characterization of recombinant 4-hydroxyphenylpyruvate dioxygenase from *Arabidopsis thaliana*, *Plant Physiol. 114*, 1587−1587.
11. Garcia, I., Rodgers, M., Lenne, C., Rolland, A., Sailland, A., and Matringe, M. (1997) Subcellular localization and purification of a *p*-hydroxyphenylpyruvate dioxygenase from cultured carrot cells and characterization of the corresponding cDNA, *Biochem. J. 325*, 761−769.
12. Wyckoff, E. E., Pishko, E. J., Kirkland, T. N., and Cole, G. T. (1995) Cloning and Expression of a Gene Encoding a T-Cell Reactive Protein from *Coccidioides-Immitis*—Homology to 4-Hydroxyphenylpyruvate Dioxygenase and the Mammalian F-Antigen, *Gene 161*, 107−111.
13. Denoya, C. D., Skinner, D. D., and Morgenstern, M. R. (1994) A *Streptomyces avermitilis* gene encoding a 4-hydroxyphenylpyruvic acid dioxygenase-like protein that directs the production of homogentisic acid and an ochronotic pigment in *Escherichia coli*, *J. Bacteriol. 176*, 5312−5319.
14. Ruetschi, U., Odelhog, B., Lindstedt, S., Barros-Soderling, J., Persson, B., and Jornvall, H. (1992) Characterization of 4-hydroxyphenylpyruvate dioxygenase. Primary structure of the *Pseudomonas* enzyme, *Eur. J. Biochem. 205*, 459−466.
15. Lindstedt, S., Odelhog, B., and Rundgren, M. (1977) Purification and some properties of 4-hydroxyphenylpyruvate dioxygenase from *Pseudomonas* sp. P. J. 874, *Biochemistry 16*, 3369−3377.
16. Serre, L., Sailland, A., Sy, D., Boudec, P., Rolland, A., Pebay-Peyroula, E., and Cohen-Addad, C. (1999) Crystal structure of *Pseudomonas fluorescens* 4-hydroxyphenylpyruvate dioxygenase: an enzyme involved in the tyrosine degradation pathway, *Struct. Fold Des. 7*, 977−988.
17. Lindstedt, S., and Rundgren, M. (1982) Blue color, metal content, and substrate binding in 4-hydroxyphenylpyruvate dioxygenase from *Pseudomonas* sp. strain P. J. 874, *J. Biol. Chem. 257*, 11922−11931.
18. Crouch, N. P., Adlington, R. M., Baldwin, J. E., Lee, M. H., and MacKinnon, C. H. (1997) A mechanistic rationalisation for the substrate specificity of recombinant mammalian 4-hydroxyphenylpyruvate dioxygenase (4-HPPD), *Tetrahedron 53*, 6993−7010.
19. Johnson-Winters, K., Purpero, V. M., Kavana, M., Nelson, T., and Moran, G. R. (2003) (4-Hydroxyphenyl)pyruvate Dioxygenase from *Streptomyces avermitilis*: The Basis for Ordered Substrate Addition, *Biochemistry 42*, 2072−2080.
20. Lindblad, B., Lindstedt, G., and Lindstedt, S. (1970) The mechanism of enzymic formation of homogentisate from *p*-hydroxyphenylpyruvate, *J. Am. Chem. Soc. 92*, 7446−7449.
21. Rundgren, M. (1982) Tritium isotope effects in the reaction catalyzed by 4-hydroxyphenylpyruvate dioxygenase from *Pseudomonas* sp. strain P. J. 874, *Biochim. Biophys. Acta 704*, 59−65.
22. Adlington, R. M., Baldwin, J. E., Crouch, N. P., Lee, M. H., and MacKinnon, C. H. (1996) Identification and stereochemistry of the product of 4-HPPD catalyzed oxidation of the ketoacid of methionine, *Bioorg. Med. Chem. Lett. 6*, 2003−2006.
23. Baldwin, J. E., Crouch, N. P., Fujishima, Y., Lee, M. H., Mackinnon, C. H., Pitt, J. P. N., and Willis, A. C. (1995) 4-Hydroxyphenylpyruvate Dioxygenase Appears to Display α-Ketoisocaproate Dioxygenase Activity in Rat Liver, *Bioorg. Med. Chem. Lett. 5*, 1255−1260.
24. Hubbard, B. K., Thomas, M. G., and Walsh, C. T. (2000) Biosynthesis of L-*p*-hydroxyphenylglycine, a nonproteinogenic amino acid constituent of peptide antibiotics, *Chem. Biol. 7*, 931−942.
25. Choroba, O. W., Williams, D. H., and Spencer, J. B. (2000) Biosynthesis of the vancomycin group of antibiotics: Involvement of an unusual dioxygenase in the pathway to (S)-4-hydroxyphenylglycine, *J. Am. Chem. Soc. 122*, 5389−5390.
26. Sheldrick, G. M., Jones, P. G., Kennard, O., Williams, D. H., and Smith, G. A. (1978) Structure of vancomycin and its complex with acetyl-D-alanyl-D-alanine, *Nature 271*, 223−225.
27. Seto, H., Fujioka, T., Furihata, K., Kaneko, I., and Takahashi, S. (1989) Structure of Complestatin, a Very Strong Inhibitor of Protease Activity of Complement in the Human-Complement System, *Tetrahedron Lett. 30*, 4987−4990.
28. Townsend, C. A., and Brown, A. M. (1983) Nocardicin A: biosynthetic experiments with amino acid precursors, *J. Am. Chem. Soc. 105*, 913−918.
29. Kempter, C., Kaiser, D., Haag, S., Nicholson, G., Gnau, V., Walk, T., Gierling, K. H., Decker, H., Zahner, H., Jung, G., and Metzger, J. W. (1997) CDA: Calcium-dependent peptide antibiotics from *Streptomyces coelicolor* A3(2) containing unusual residues, *Angew. Chem. Int. Ed. Eng. 36*, 498−501.
30. Ciabatti, R., Kettenring, J. K., Winters, G., Tuan, G., Zerilli, L., and Cavalleri, B. (1989) Ramoplanin (A-16686), a new glycolipodepsipeptide antibiotic. III. Structure elucidation, *J. Antibiot. (Tokyo) 42*, 254−267.
31. van Wageningen, A. M., Kirkpatrick, P. N., Williams, D. H., Harris, B. R., Kershaw, J. K., Lennard, N. J., Jones, M., Jones, S. J., and Solenberg, P. J. (1998) Sequencing and analysis of genes involved in the biosynthesis of a vancomycin group antibiotic, *Chem. Biol. 5*, 155−162.
32. Hojati, Z., Milne, C., Harvey, B., Gordon, L., Borg, M., Flett, F., Wilkinson, B., Sidebottom, P. J., Rudd, B. A., Hayes, M. A., Smith, C. P., and Micklefield, J. (2002) Structure, Biosynthetic Origin, and Engineered Biosynthesis of Calcium-Dependent Antibiotics from *Streptomyces coelicolor*, *Chem. Biol. 9*, 1175−1187.
33. Pelzer, S., Sussmuth, R., Heckmann, D., Recktenwald, J., Huber, P., Jung, G., and Wohlleben, W. (1999) Identification and analysis of the balhimycin biosynthetic gene cluster and its use for manipulating glycopeptide biosynthesis in *Amycolatopsis mediterranei* DSM5908, *Antimicrob. Agents Chemother. 43*, 1565−1573.
34. Chiu, H. T., Hubbard, B. K., Shah, A. N., Eide, J., Fredenburg, R. A., Walsh, C. T., and Khosla, C. (2001) Molecular cloning and sequence analysis of the complestatin biosynthetic gene cluster, *Proc. Natl. Acad. Sci. U.S.A. 98*, 8548−8553.
35. Price, J. C., Barr, E. W., Tirupati, B., Bollinger, J. M., Jr., and Krebs, C. (2003) The first direct characterization of a high-valent iron intermediate in the reaction of an α-ketoglutarate-dependent dioxygenase: a high-spin Fe(IV) complex in taurine/α-ketoglutarate dioxygenase (TauD) from *Escherichia coli*, *Biochemistry 42*, 7497−7508.
36. McGuffin, L. J., Bryson, K., and Jones, D. T. (2000) The PSIPRED protein structure prediction server, *Bioinformatics 16*, 404−405.
37. Thompson, J. D., Gibson, T. J., Plewniak, F., Jeanmougin, F., and Higgins, D. G. (1997) The CLUSTAL_X windows interface: flexible strategies for multiple sequence alignment aided by quality analysis tools, *Nucleic Acids Res. 25*, 4876−4882.
38. Kimura, M. (1983) *The Neutral Theory of Molecular Evolution*, Cambridge University Press, New York.
39. Saitou, N., and Nei, M. (1987) The neighbor-joining method: a new method for reconstructing phylogenetic trees, *Mol. Biol. Evol. 4*, 406−425.
40. Page, R. D. (1996) TreeView: an application to display phylogenetic trees on personal computers, *Comput. Appl. Biosci. 12*, 357−358.
41. Ho, S. N., Hunt, H. D., Horton, R. M., Pullen, J. K., and Pease, L. R. (1989) Site-directed mutagenesis by overlap extension using the polymerase chain reaction, *Gene 77*, 51−59.
42. Lee, M. H., Zhang, Z. H., MacKinnon, C. H., Baldwin, J. E., and Crouch, N. P. (1996) The C-terminal of rat 4-hydroxyphenylpyruvate dioxygenase is indispensable for enzyme activity, *FEBS Lett. 393*, 269−272.
43. Que, L., Jr., and Ho, R. Y. (1996) Dioxygen Activation by Enzymes with Mononuclear Non-Heme Iron Active Sites, *Chem. Rev. 96*, 2607−2624.

44. Hogan, D. A., Smith, S. R., Saari, E. A., McCracken, J., and Hausinger, R. P. (2000) Site-directed mutagenesis of 2,4-dichlorophenoxyacetic acid/α-ketoglutarate dioxygenase. Identification of residues involved in metallocenter formation and substrate binding, *J. Biol. Chem. 275*, 12400−12409.
45. Lindstedt, S., and Rundgren, M. (1982) Inhibition of 4-hydroxyphenylpyruvate dioxygenase from *Pseudomonas* sp. strain P. J. 874 by the enol tautomer of the substrate, *Biochim. Biophys. Acta 704*, 66−74.
46. Holme, E., Linstedt, S., and Nordin, I. (1982) Uncoupling in the γ-butyrobetaine hydroxylase reaction by D- and L-carnitine, *Biochem. Biophys. Res. Commun. 107*, 518−524.
47. Hsu, C. A., Saewert, M. D., Polsinelli, L. F., Jr., and Abbott, M. T. (1981) Uracil's uncoupling of the decarboxylation of α-ketoglutarate in the thymine 7-hydroxylase reaction of *Neurospora crassa*, *J. Biol. Chem. 256*, 6098−6101.
48. Salowe, S. P., Marsh, E. N., and Townsend, C. A. (1990) Purification and characterization of clavaminate synthase from *Streptomyces clavuligerus*: an unusual oxidative enzyme in natural product biosynthesis, *Biochemistry 29*, 6499−6508.
49. Pavel, E. G., Zhou, J., Busby, R. W., Gunsior, M., Townsend, C. A., and Solomon, E. I. (1998) Circular dichroism and magnetic circular dichroism spectroscopic studies of the non-heme ferrous active site in clavaminate synthase and its interaction with α-ketoglutarate cosubstrate, *J. Am. Chem. Soc. 120*, 743−753.
50. Valegard, K., van Scheltinga, A. C., Lloyd, M. D., Hara, T., Ramaswamy, S., Perrakis, A., Thompson, A., Lee, H. J., Baldwin, J. E., Schofield, C. J., Hajdu, J., and Andersson, I. (1998) Structure of a cephalosporin synthase, *Nature 394*, 805−809.
51. Elkins, J. M., Ryle, M. J., Clifton, I. J., Dunning Hotopp, J. C., Lloyd, J. S., Burzlaff, N. I., Baldwin, J. E., Hausinger, R. P., and Roach, P. L. (2002) X-ray crystal structure of *Escherichia coli* taurine/α-ketoglutarate dioxygenase complexed to ferrous iron and substrates, *Biochemistry 41*, 5185−5192.
52. Zhou, J., Gunsior, M., Bachmann, B. O., Townsend, C. A., and Solomon, E. I. (1998) Substrate binding to the α-ketoglutarate-dependent non-heme iron enzyme clavaminate synthase 2: Coupling mechanism of oxidative decarboxylation and hydroxylation, *J. Am. Chem. Soc. 120*, 13539−13540.
53. Rundgren, M. (1977) Steady-state kinetics of 4-hydroxyphenylpyruvate dioxygenase from human liver (III), *J. Biol. Chem. 252*, 5094−5099.
54. Solomon, E. I., Brunold, T. C., Davis, M. I., Kemsley, J. N., Lee, S. K., Lehnert, N., Neese, F., Skulan, A. J., Yang, Y. S., and Zhou, J. (2000) Geometric and electronic structure/function correlations in non-heme iron enzymes, *Chem. Rev. 100*, 235−350.
55. Goodwin, S., and Witkop, B. (1957) Quinol Intermediates in the Oxidation of Phenols and Their Rearrangements, *J. Am. Chem. Soc. 79*, 179−185.
56. Hamilton, G. A. (1971) The proton in biological redox reactions, *Prog. Bioorg. Chem. 1*, 83−152.
57. Jefford, C. W. (1992) Non-heme dioxygenases: A unified mechanistic interpretation of their mode of action, *Adv. Det. React. Mech. 2*, 149−187.
58. Niederwieser, A., Wadman, S. K., and Danks, D. M. (1978) Excretion of *cis*- and *trans*-4-hydroxycyclohexylacetic acid in addition to hawkinsin in a family with a postulated defect of 4-hydroxyphenylpyruvate dioxygenase, *Clin. Chim. Acta 90*, 195−200.
59. Meister, A., and Anderson, M. E. (1983) Glutathione, *Annu. Rev. Biochem. 52*, 711−760.
60. Forbes, B. J. R., and Hamilton, G. A. (1994) Mechanism and Mechanism-Based Inactivation of 4-Hydroxyphenylpyruvate Dioxygenase, *Bioorg. Chem. 22*, 343−361.
61. Pascal, R. A., Jr., Oliver, M. A., and Chen, Y. C. (1985) Alternate substrates and inhibitors of bacterial 4-hydroxyphenylpyruvate dioxygenase, *Biochemistry 24*, 3158−3165.
62. Ryle, M. J., and Hausinger, R. P. (2002) Non-heme iron oxygenases, *Curr. Opin. Chem. Biol. 6*, 193−201.
63. Jennings, W. B., Rutherford, M., Agarwal, S. K., Boyd, D. R., Malone, J. F., and Kennedy, D. A. (1986) Conformation and stereodynamics of the oxepine ring-system, *J. Chem. Soc., Chem. Commun.*, 970−972.
64. Vogel, E., and Gunther, H. (1967) Benzene oxide-Oxepin Valence Tautomerism, *Angew. Chem., Int. Ed. Engl. 6*, 385.
65. Lowry, T. H., and Richardson, K. S. (1987) *Mechanism and Theory in Organic Chemistry*, 3rd ed., Harper and Row, New York.
66. Pollack, R. M., Mack, J. P. G., and Blotny, G. (1987) Ketonization of 1,3-Cyclohexadienol, a Conjugated Enol, *J. Am. Chem. Soc. 109*, 3138−3139.
67. Dzingeleski, G. D., Bantia, S., Blotny, G., and Pollack, R. M. (1988) Kinetics and Mechanism of the Ketonization of a Conjugated Trienol, *J. Org. Chem. 53*, 1540−1544.
68. Fairley, D. J., Boyd, D. R., Sharma, N. D., Allen, C. C., Morgan, P., and Larkin, M. J. (2002) Aerobic Metabolism of 4-Hydroxybenzoic Acid in Archaea via an Unusual Pathway Involving an Intramolecular Migration (NIH Shift), *Appl. Environ. Microbiol. 68*, 6246−6255.

BI035762W